



# Production of renewable mesitylene as jet-fuel additive: Reaction kinetics of acetone self-condensation over basic (TiO<sub>2</sub>) and acid (Al-MCM-41) catalysts

Adrián García, Pablo Marín, Salvador Ordóñez\*

Catalysis, Reactors and Control Research Group (CRC), Dept. of Chemical and Environmental Engineering, University of Oviedo, Julián Clavería 8, Oviedo 33006, Spain

## ARTICLE INFO

### Keywords:

1,3,5-trimethylbenzene  
Condensation  
Dehydration  
Reaction mechanism  
Aluminosilicate catalysts

## ABSTRACT

Sustainable production of jet fuel additives plays an essential role to decrease greenhouse gas emissions in the aviation industry. Acetone obtained from biomass fermentation is one of the platform molecules of the bio-refinery that can be used as raw material of newly developed sustainable processes. Mesitylene jet fuel additive can be obtained by acetone self-condensation reaction catalyzed by porous solids. In the present work, TiO<sub>2</sub> and Al-MCM-41 have been chosen, respectively, as basic and acid catalysts, because of having some tolerance to deactivation. The reaction was studied in a continuous fixed-bed reactor operated in the gas phase at space velocities of 7900 mol/kg h for TiO<sub>2</sub> and 5000 mol/kg h for Al-MCM-41. The influence of feed concentration (5–20% acetone and 0–5% mesityl oxide) and temperature (200–350 °C) was studied. First, the reaction scheme was assessed based on the product distribution. It was found that the acid catalyst Al-MCM-41 favors mesityl oxide decomposition to undesired isobutylene and acetic acid. Then, a mechanistic kinetic model of the different steps of the reaction scheme was developed and fitted the experimental results of each catalyst. This model constitutes a valuable tool for the scale-up of this process.

## 1. Introduction

The implementation of a sustainable circular economy model is one of the current major objectives in most industrialized countries [1]. The use of biomass for the production of chemicals and fuels will be one of the basis for achieving this objective [2]. In this context, the aviation industry is claimed to experience an important change in the following years and decades to reduce the emissions of greenhouse gases (GHG). Air traffic is continuously growing, and it is not expected to stabilize or decrease in the near future. Despite reductions in flying during the Covid-19 lockdowns, 2% of global energy-related CO<sub>2</sub> emissions were caused by aviation in 2022. Moreover, CO<sub>2</sub> emissions from aviation have reached 80% of their pre-pandemic peak, with >800 Mt. CO<sub>2</sub>, a value which is expected to grow rapidly [3].

The 184 member states of the International Civil Aviation Organization (ICAO) adopted in 2022 a long-term global aspirational goal of net zero carbon emissions from international aviation by 2050. To achieve this goal, bio-based aviation fuels can provide significant reductions in greenhouse gas emissions caused by petroleum-derived fuels. Depending on the technique applied to produce the biofuels, the

greenhouse gas emissions may decrease between 41 and 89% [4]. Carbon emissions reduction is not the only driver for aviation biofuels, energy security is also an important benefit of biofuels, since they can be produced everywhere, reducing the oil imports [5].

Different technologies are being developed and evaluated to produce jet biofuels. Some constraints limit the applicability of these alternatives, such as, the competence with food market, which increases the food cost, low process yields, high energy demand or the absence of investment and a stable sustainable raw materials supply [4,5]. Despite this, some aviation biofuels are close to be commercialized, the hydro-processed esters and fatty acids (HEFA) fuel, Fisher-Tropsch (FT) fuel and pyrolysis fuel. In the case of HEFA fuel, GHG emissions are produced during fuel production, but also because of the use of fertilizers to promote crops growing, causing the lowest reduction among the alternatives, with a maximum value of 63% compared with a common jet fuel [6,7]. FT fuel and syngas-based higher alcohols can be produced using corn stover as biomass source, due to the low impact it causes in land, with GHG emissions reduction of 89% [8–10]. Pyrolysis fuel is produced by fast pyrolysis to pyrolysis oil, which is, then, hydrotreated and refined to obtain the fuel. GHG reduction of this alternative is 76%

\* Corresponding author.

E-mail address: [sordonez@uniovi.es](mailto:sordonez@uniovi.es) (S. Ordóñez).

<https://doi.org/10.1016/j.fuproc.2023.108007>

Received 13 October 2023; Received in revised form 15 November 2023; Accepted 21 November 2023

Available online 30 November 2023

0378-3820/© 2023 The Authors. Published by Elsevier B.V. This is an open access article under the CC BY-NC-ND license (<http://creativecommons.org/licenses/by-nc-nd/4.0/>).

[4,10].

Quality specifications for jet fuels are very strict, especially in terms of energy-density (to maximize the distance travelled by the plane) and freezing point values (to avoid crystallization at high altitudes). For this reason, the biofuel obtained is not the final product, since additives are required to fulfill the different specifications. These specifications are amply covered by branched and cyclic petroleum-derived hydrocarbons, like mesitylene, which improves the security and stability of jet fuels (e. g., RP3 fuel) [11,12]. The present work addresses the production of mesitylene jet fuel additive from biomass-derived acetone.

Mesitylene belongs to the polymethylbenzene family with multiple applications [13], such as, jet fuel additive [11], the synthesis of 2,4,6-trimethylaniline [14] (used to manufacture dyes), reactant in the fine chemical industry (to synthesize antioxidants, nitro mesitylene, etc. [15]) and other innovative applications, like Cu (II) detection in aqueous media [16].

Mesitylene can be found in coal tar oil, from which it can be isolated by distillation and purified by differential hydrolysis. Nowadays, the main industrial production is as by-product of crude oil processing, specifically in cracking and reforming operations [14,17,18]. Moreover, it can be produced by Friedel-Crafts methylation of toluene and xylene with chloromethane in the presence of aluminium chloride catalyst [19]. Lastly, it can also be generated by the reaction of toluene with synthesis gas, catalyzed by metal oxide on aluminium silicate [20]. These processes are far from being renewable and environmentally friendly, due to the use of fossil fuel feedstocks and chlorine-containing compounds.

The production of mesitylene by acetone self-condensation opens the possibility for an environmentally friendly route [21]. Acetone has been proposed as platform molecule to integrated production processes into a circular economy. Nowadays, acetone is co-produced together with phenol from oil feedstocks in the cumene process [22]. However, in the following years, the aim is to progressively replace fossil feedstocks by renewable ones. In this context, acetone can be obtained, together with butanol and ethanol, by fermentation of agriculture waste in the so-called ABE process [23]. Also, other renewable production routes have been proposed based on the pyrolysis of biomass [24] or the reaction of eggshells with acetic acid [25]. Using this type of respectful and renewable processes makes acetone become a valuable environmentally friendly platform intermediate.

Acetone self-condensation to mesitylene is a multiple-step reaction process, based on a sequence of condensation and dehydration reaction stages [26]. In the gas phase, this reaction can be catalyzed by acid or basic solid catalysts. Basic catalysts promote the formation of phorone intermediates, while acid catalysts are able to accomplish the complete condensation to mesitylene [27]. However, acid catalysts have some drawbacks, due to the formation of acetic acid and isobutene in a side reaction ( $\beta$ -scission of C6 compounds), which is responsible of a fast initial catalyst deactivation [26].

Previous works demonstrated that different acid catalysts are active in mesitylene synthesis. HZSM-5 zeolite requires too high reaction temperature, which promotes a critical catalyst deactivation [28]. HY-5 zeolite requires moderate temperature (200–300 °C) and high pressure (75 bar) to obtain mesitylene yields of ca. 12% [2].  $\beta$ -zeolite and Al-MCM-41 have also been studied with interesting results for the case of Al-MCM-41; for the  $\beta$ -zeolite, isobutene is the main product, due to the strong acidity of this catalyst [29]. Different studies about the steps of the reaction with acid catalysts have been published. Thus, Huber et al. (2023) [30] studied the mechanism of the  $\beta$ -scission reaction and the reverse reaction over acid catalysts (H-SSZ-13 zeolite). Hermann et al. (2017) [31] studied the mechanism of acetone condensation to mesityl oxide using different aluminosilicate catalyst; they proposed the addition of Pt to the catalyst and H<sub>2</sub> to the feed stream to avoid the observed fast deactivation of the catalyst. Kumar et al. (2004) [32] studied the step of isophorone dehydration to mesitylene over Al<sub>2</sub>O<sub>3</sub> finding that moderate acidity of the catalyst is required to obtain mesitylene, but a

strong acidity favors isophorone decomposition to linear compounds. Among all the catalyst studied, Al-MCM-41 showed the best behavior regarding deactivation [29]. This moderate acid catalyst exhibited high selectivity to mesitylene, especially in the lower temperature range, and less isobutylene generation, because of its moderate acidity.

Basic catalysts have also been studied. Their main drawback is deactivation at high temperature, caused by adsorption of high molecular weight oligomers [33]. Different authors tried to solve this problem in different ways, such as, synthesizing alkali-promoted MgO catalysts, with undesired results [34]. Other authors studied Li and Rb doped-TiO<sub>2</sub> and observed that a strong basicity is responsible of a higher mesitylene selectivity [35]. TiO<sub>2</sub>, MgO and MgAl have also been studied and compared in the temperature range of 200–450 °C and pressure of 2.5 bar [29], being TiO<sub>2</sub> the catalyst with the best performance. For this catalyst, mesityl oxide was the main product, while the other ones presented high selectivity to phorones and isophorones.

The selection of a suitable catalyst, able to maximize mesitylene production with tolerance to deactivation, is the key to ensure the process viability. Previous works were focused on the development of suitable catalysts for this reaction. It was found that acid and basic catalysts exhibit quite different behavior in terms of product selectivity, which is not optimum due to the formation of many side products. In this work, an acid catalyst, Al-MCM-41, and a basic one, TiO<sub>2</sub>, have been selected. Both catalysts can operate within the same pressure (2.5 bar) and temperature range (250–300 °C) with good activity. Hence, these catalysts may be combined as a mechanical mixture, either as a single fixed-bed or in two consecutive fixed-beds, to exploit their advantages and face their limitations. To answer this question detailed knowledge of the reaction scheme and the corresponding reaction kinetics is needed, and the aim of the present work is to obtain this information. First, the reaction pathway of the acid and basic catalysts has been determined by means of experiments carried out in a fixed-bed reactor. Then, the catalyst stability has been studied and the main deactivation causes identified. Finally, a mechanistic kinetic model has been proposed for each catalyst and fitted to the results of the kinetic experiments carried out at different reactant concentration and temperature.

The kinetics models, proposed in this work for the first time for this reaction, are critical to accomplish the reactor scale-up to a commercial process. The most efficient combination of both catalysts and the optimum operating conditions can be determined in order to maximize mesitylene yield.

## 2. Materials and methods

### 2.1. Materials

Two commercial catalysts are used: anatase TiO<sub>2</sub> 1/8" pellets (VWR) and H-Al-MCM-41 (Si/Al = 39.5, Aldrich, 643,653). Both catalysts were sieved to obtain particles in the range 100–350  $\mu$ m. Thermal pre-treatments in an air stream are applied to both catalysts before the reaction: TiO<sub>2</sub> was pre-treated by heating from 20 to 450 °C at 10 °C/min (hold at 450 °C for 3 h) and Al-MCM-41 from 20 to 550 °C at 1 °C/min (hold at 550 °C for 12 h).

Chemical reagents are the following: acetone ( $\geq$ 99.9%, VWR), mesityl oxide (technical grade, 90%, Aldrich), isophorone (98%, Acros Organics), mesitylene (extra pure, 99%, Acros Organics), acetic acid ( $\geq$ 99.8%, ACS) and nitrogen (Air Liquide).

### 2.2. Catalyst characterization

Micromeritics ASAP 2020 was used to measure the textural properties of fresh and used catalysts by N<sub>2</sub> physisorption (before the analysis the samples were degasified at 10 mmHg and 250 °C). Micropore volume and specific surface area were determined by the t-plot method, mesopore volume and size were measured by Barrett-Joyner-Halenda (BJH) method using the Kelvin model of pore filling, and the total

surface area was calculated by Brunauer-Emmett-Teller (BET) method.

Temperature-programmed oxidation (TPO) analyses were carried out in a Micromeritics Autochem II 2920 to reveal the presence of organic compounds deposited on the catalysts. The analysis was divided in different parts: cleaning with helium (20 mL/min) at 5 °C/min heating rate up to 150 °C for 30 min, and oxidation in a 5% O<sub>2</sub> in helium stream (20 mL/min) at a 2.5 °C/min heating rate up to 950 °C. The effluent was analyzed on-line using a mass spectrometer (Omnistar GSD 301).

### 2.3. Experimental device

Reactions were carried out in the gas phase using a continuous fixed-bed reactor. The reactor consisted of a stainless-steel tube (8.32 mm of inside diameter and 600 mm length) loaded with the catalyst sieved to a particle size of 100–350 μm (0.5 g of Al-MCM-41 or 1 g of TiO<sub>2</sub>). To avoid channelling and ensure a piston flow pattern, the ratio of reactor diameter to solid particle size was higher than 10 (33) and the ratio of bed length to solid particle size was higher than 50 (> 66 for Al-MCM-41 and, for the case of TiO<sub>2</sub>, the catalyst particles were mixed with glass particles of the same size to achieve this requirement) [36]. A stainless-steel mesh was used as support, on top of which a small bed of glass spheres (1 g and 100–350 μm of particle size) was placed to provide uniform support for the catalyst particles. Above the catalyst bed, the reactor was filled with glass spheres (1 mm) to ensure uniform flow distribution and avoid channelling.

Temperature inside the reactor was kept constant using a PID-controlled oven and a K-type thermocouple located inside the reactor tube downstream the catalytic bed.

The reactor feed was a gas stream of the reactants (acetone or mesityl oxide) in nitrogen carrier. The reactants were introduced as liquids using a HPLC pump (Teledyne SSI LAB ALLIANCE Series II), mixed with the nitrogen stream and vaporized with the help of a heating tape maintained at 180 °C. The flow rate of nitrogen (0.35–2.7 NL/min) was set using a mass flow controller (BRONKHORST). The concentration of reactant and total feed flow rate were varied independently by adjusting the liquid and gas flow rates. The reactor absolute pressure was set to 280 kPa for all experiments using a valve placed at the outlet of the reactor tube. A sketch of the experimental device is depicted in Fig. 1.

The reactor gas outflow was analyzed on-line using a gas chromatograph (GC, AGILENT HP-6890 N), equipped with a HP Plot Q column to separate reactants and products, and a flame ionization (FID) detector. Peak identification and response areas were assessed using commercial standards. Some samples were taken from the reactor effluent for off-line analysis in a gas chromatograph equipped with a

mass spectrometer detector (GC–MS) to determine the structure of the reaction intermediates.

The concentration of the reactor effluent was used to determine the reactant conversion and product selectivity using the following expressions:

$$\text{Reactant conversion} = \frac{\sum n_j (x_{j,in} - x_{j,out})}{\sum n_j x_{j,in}} \quad (1)$$

$$\text{Product selectivity} = \frac{n_i x_i}{\sum n_j (x_{j,in} - x_{j,out})} \quad (2)$$

Where,  $x_j$  and  $x_i$  are, respectively, the molar fractions in the reactor outflow of the  $j$  reactant and the  $i$  product, and  $n_i$  is the number of carbon atoms in the molecule.

### 2.4. Reaction tests

The stability studies have been carried to measure the stability of the catalysts upon time. In these studies, the reactor temperature (275 °C) and feed (WHSV = 1900 mol/kg h for TiO<sub>2</sub> and WHSV = 2800 mol/kg h for Al-MCM-41) were maintained constant and the reactor effluent was analyzed continuously for a period of 8 to 15 h.

The kinetic studies have been done to evaluate the influence of concentration and temperature on the reaction rates. The feed concentration of the reactants, acetone (5–20 mol%) or mesitylene oxide (1–5 mol%), and the reactor temperature (200–360 °C) were varied. Total pressure (280 kPa) was maintained constant. For each set of conditions, once the steady state was reached in the reactor, the reactor gas outflow was analyzed. The total gas flow rate was adjusted to maintain conversion below 10% at all the tested conditions. By this way, the reactant and product rates of reaction were calculated using the differential reactor model (i.e., concentration and temperature being the same for all the catalyst particles):

$$r_i = \frac{dF_i}{dW} \approx \frac{F_i - F_{i0}}{W} = \frac{F_0}{W} (x_i - x_{i0}) \quad (3)$$

Where  $r_i$ ,  $F_i$  and  $x_i$  are, respectively, the reaction rate, the molar flow rate and the molar fraction of compound  $i$ ,  $W$  is the catalyst weight and  $F_0/W$  is the space velocity (WHSV).

## 3. Results and discussion

### 3.1. Reaction pathway

The evaluation of the reactor outflow showed that the main products

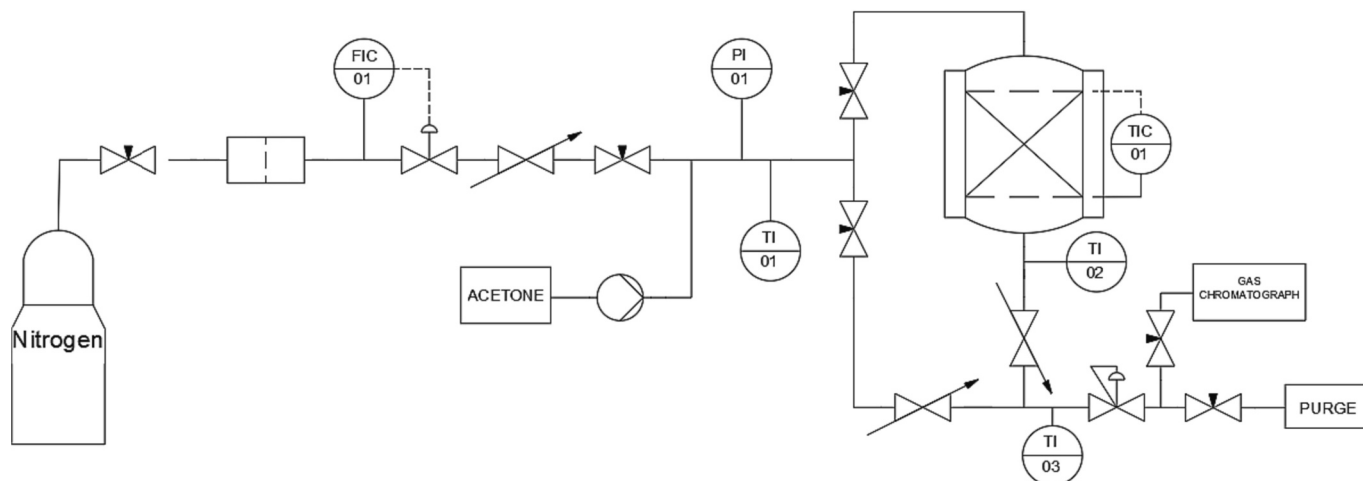


Fig. 1. Experimental set-up used for the reaction experiments performed in this work.

obtained in this reaction were mesityl oxide, phorones, isophorones, mesitylene, and the non-desired products of isobutylene, acetic acid and CO<sub>2</sub>. These compounds were identified by GC-MS and quantified by GC-FID. The product distribution can be analyzed in Fig. 2 as a function of reactant conversion. These tests were performed using as reactants acetone alone and a mixture of acetone and mesityl oxide.

For the TiO<sub>2</sub> catalyst, the tests carried out with acetone alone as reactant (Fig. 1a) showed that on increasing conversion, the selectivity of mesityl oxide decreased, while the selectivity of isophorone and mesitylene increased. This behavior suggests, as depicted in Fig. 3, a reaction scheme in series to phorone with mesityl oxide being the reaction intermediate (reactions 1 and 2), followed by the formation in parallel of mesitylene (reaction 3) and isophorone (reaction 5) final products. Phorone selectivity was very low, compared to the other intermediates and final products. This fact suggests that phorones react very fast to produce isophorones and mesitylene ( $r_2 \approx r_3 + r_5$ ). For the case of using as reactants a mixture of acetone and mesityl oxide (Fig. 2b), it was observed that part of mesityl oxide decomposed to acetone, what confirms that the self-condensation of acetone to mesityl oxide (reaction 1) is a reversible reaction [30]. In addition, a little selectivity to isobutylene was reported at high conversion, attributed to the  $\beta$ -scission side reaction of mesityl oxide (reaction 4). However, this route can be considered almost negligible for the TiO<sub>2</sub> catalyst. The behavior of mesitylene and isophorone with this reactant mixture is similar with the difference that, in this case, phorone intermediate was detected. Thus, the higher concentration of mesityl oxide may lead to higher reaction rates to phorone (reaction 2), being now within the same order of magnitude as the reaction rates to mesitylene and isophorone ( $r_2 \sim r_3 < r_5$ ).

The behavior of the Al-MCM-41 was quite different. When using acetone alone as the reactant (Fig. 2c), isobutylene was the main product, followed by mesitylene. For acid catalysts, an important

fraction of the formed mesityl oxide decomposed to isobutylene and acetic acid (reaction 4), which is the main undesired reaction of the reaction scheme (Fig. 3). Intermediates like mesityl oxide, phorones and isophorones had low selectivity, particularly at high conversion, suggesting that the step with the lowest reaction rate was acetone self-condensation (reaction 1). When using a mixture of acetone and mesityl oxide as reactants (Fig. 2d), isobutylene selectivity was kept low at low conversion, but it raised considerably at high conversion. This behavior is explained by the competition between  $\beta$ -scission (reaction 4) and condensation (reaction 2) parallel reactions of mesityl oxide (Fig. 3). The  $\beta$ -scission reaction requires water as reactant, but the only source of water is as product in the condensation mesityl oxide. For this reason, at high mesityl oxide conversion, the availability of water is higher and the rate of  $\beta$ -scission reaction increases. Conversely, when acetone alone is used as a reactant, the first step of the reaction scheme (Fig. 3) is the condensation to mesityl oxide with release of one water molecule. This guarantees excess of water for the  $\beta$ -scission reaction and, hence, selectivity of isobutylene is high even at low conversions.

In this case, phorones were detected, but with low concentration. Differently from the observations with the TiO<sub>2</sub> catalyst, isophorone selectivity exhibited a decreasing trend with conversion. This is in agreement with the occurrence of isophorone dehydration to mesitylene, which is possible in acid catalysts [29].

### 3.2. Catalyst stability

The stability of the catalysts upon time was evaluated at 275 °C using fresh catalysts and a feed made of nitrogen gas carrier containing 15% acetone or a mixture of 5% acetone and 5% mesityl oxide. The space velocity (WHSV) was 1900 mol/kg h for TiO<sub>2</sub>, and 100 mol/kg h (feed of acetone alone) or 900 mol/kg h (test with mixture of acetone and mesityl oxide) for Al-MCM-41. The methodology followed was detailed

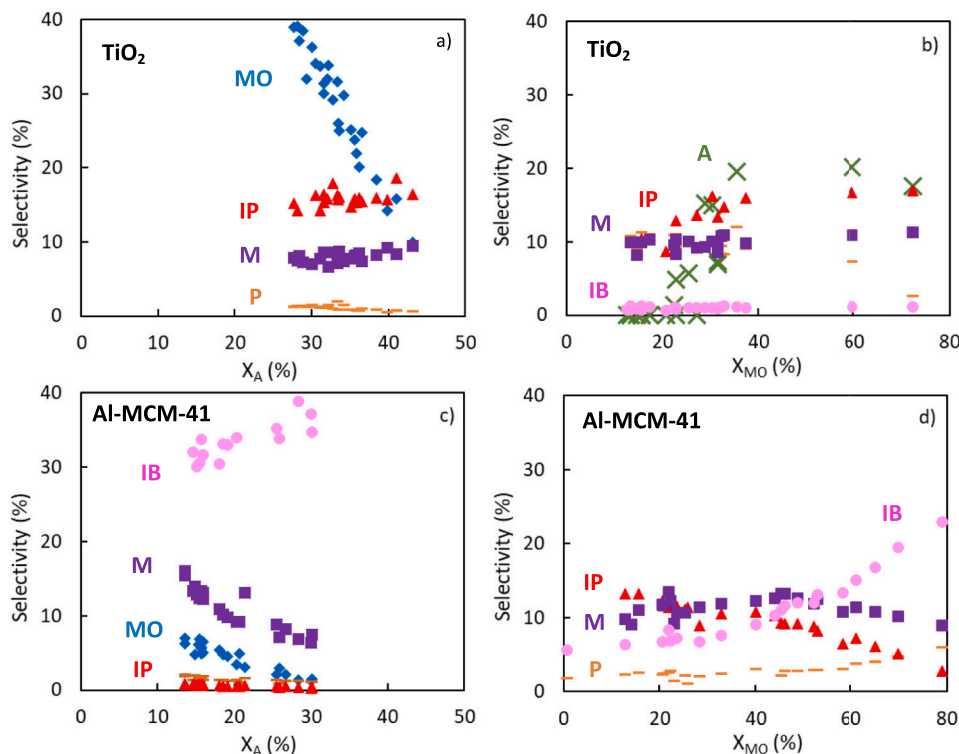


Fig. 2. Product selectivity distribution for experiments using acetone and mesityl oxide mixed with acetone as the reactants and TiO<sub>2</sub> (a), (b) and Al-MCM-41 (c) and (d) as the catalysts respectively. Legend: acetone (X), mesityl oxide (◆), phorone (—), isophorone (▲), mesitylene (■), isobutylene (●) are represented.

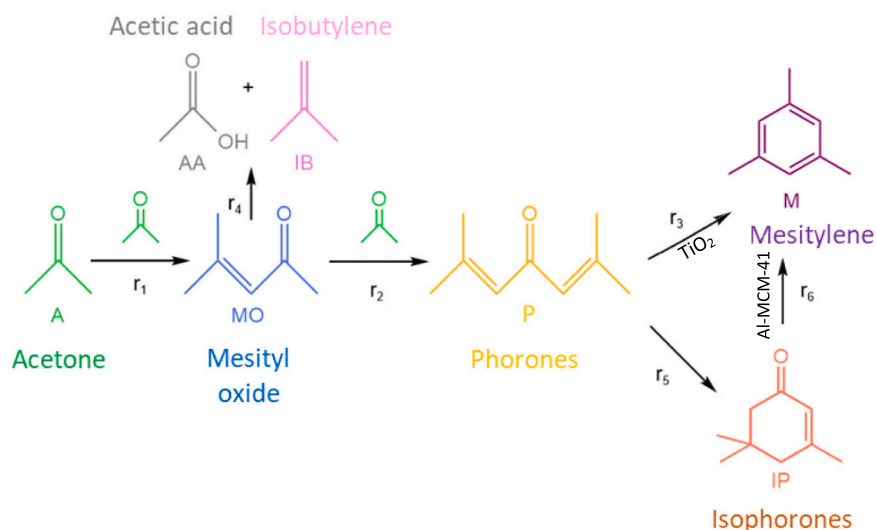


Fig. 3. Reaction scheme for mesitylene synthesis using acetone as the reactant.

in Section 2.4. In every test, the reactor was operated for the time required to achieve stable reaction conditions, measured in terms of conversion.

The performance of both catalysts is compared in Fig. 4. Fig. 4a shows the evolution of conversion when using as reactant acetone alone. Both catalysts exhibited a progressive drop in conversion during the first 5 h of reaction, attributed to catalyst deactivation. Then, conversion reached a stable value of 30% for  $\text{TiO}_2$  and 16% for Al-MCM-41. Fig. 4b displays a similar graph, but for the case of using a mixture of acetone and mesityl oxide as reactants. In this case, the initial conversion was higher, but it dropped to similar values as in the previous test, 17% for  $\text{TiO}_2$  and 25% for Al-MCM-41. It also took more time to reach these values, around 8 h.

Fig. 5 analyses how the catalyst deactivation influenced the product distribution. For the  $\text{TiO}_2$  catalyst and acetone alone as reactant (Fig. 5a), after the stabilization, the yield of the end-products decreased: mesitylene changed from 9.5% to 2.1% and isophorone from 7.1% to 4.0%. This decrease was accompanied by an increase in the yield of mesityl oxide intermediate, from 4.3% to 11.0%. These findings agree with a decrease in acetone conversion for a reaction scheme in series (Fig. 2): the intermediate (mesityl oxide) increased in selectivity or yield, while the final products decreased.

The stability of the catalysts was also studied when using a mixture of acetone and mesityl oxide as reactants (Fig. 5b). For  $\text{TiO}_2$ , acetone was produced due to mesityl oxide hydrolysis, which is particularly relevant at the beginning of the experiment (yield of acetone 12.7%). This reaction turned negligible after the stabilization of the catalyst since

conversion and the yield of all the products decreased considerably. The product distribution also changed, being isophorone the main reaction product, followed by mesitylene. In addition, phorone intermediates appeared with yields of 1.9% and 1.7%, after the stabilization.

For the Al-MCM-41 catalyst, the product distribution was completely different (Fig. 5a). The main product was isobutylene, which is a consequence of the  $\beta$ -scission of mesityl oxide side reaction (Fig. 3, reaction 4). After the stabilization of the catalyst, isobutylene suffered a drop in yield from 11% to 4.9%; nevertheless, it continued to be the main product. Mesitylene yield remained constant to 2%, even though acetone conversion decreased. Mesityl oxide yield increased to 1%. This suggests that reaction rates of mesityl oxide to isobutylene and phorones (and mesitylene) were affected in a different way by the loss of catalyst activity. For the case of a mixture of acetone and mesityl oxide as reactants, it is observed an increase in the yield of mesitylene with respect the case of acetone alone (from 2% to 4.9%, before the stabilization). Also, the yields of mesitylene and isophorone increased, which points to an increase in the rates of the condensation path, in detriment of the  $\beta$ -scission one.

The sum of the compound yields of Fig. 5 is lower than the corresponding to acetone or mesityl oxide conversion (e.g. the sum of the selectivity in lower than 100%). This is due to the adsorption on the catalyst surface of the different products and intermediates and it is responsible of the observed deactivation during the stability studies.

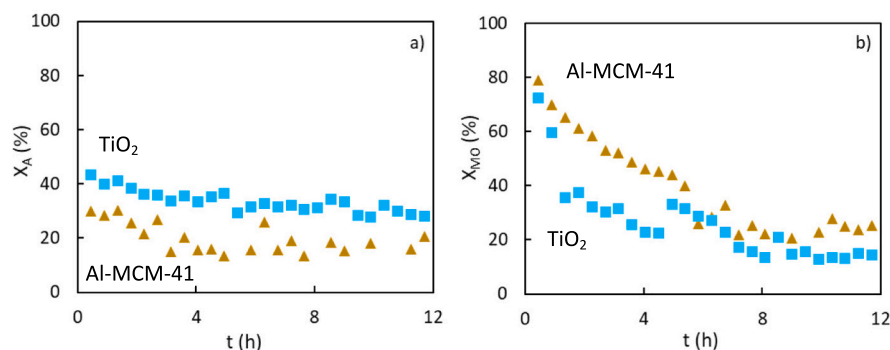


Fig. 4. Stability study at 275 °C. Reactants: (a) 15% acetone and (b) mixture of acetone and mesityl oxide (5% each one). Catalysts:  $\text{TiO}_2$  (■), Al-MCM-41 (▲).

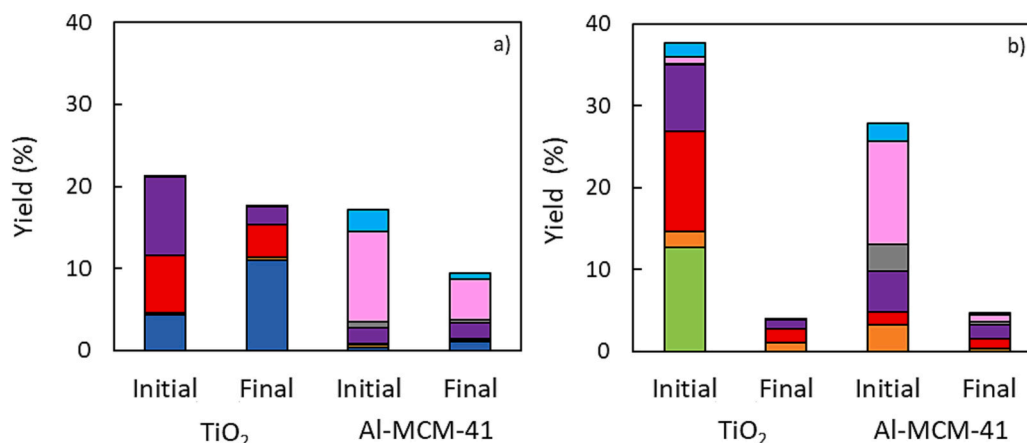


Fig. 5. Product yield distribution before and after the stabilization at 275 °C for (a) acetone alone and (b) mixture of acetone and mesityl oxide. Legend: acetone (■), mesityl oxide (■), phorone (■), isophorone (■), mesitylene (■), acetic acid (■), isobutylene (■) and CO<sub>2</sub> (■).

### 3.3. Catalyst characterization

The acidity and basicity of the catalysts were determined in the scope of previous works [29] by temperature-programmed-desorption (TPD) of NH<sub>3</sub> and CO<sub>2</sub>, respectively. TiO<sub>2</sub> exhibited a moderate concentration of basic sites (0.24 mmol CO<sub>2</sub>/g) and a very low concentration of acid sites (0.03 mmol NH<sub>3</sub>/g). Conversely, the basicity of Al-MCM-41 was low, 0.1 mmol CO<sub>2</sub>/g, while the acidity with a value of 1.09 mmol NH<sub>3</sub>/g was considerably high, due to the insertion of Al in the structure of the MCM-41.

Nitrogen adsorption analysis is showed in Table 1. After the stability study, surface area and pore volume of the catalysts decreased, particularly for the Al-MCM-41. The decrease in surface area is accompanied by a decrease in activity, as observed during the stability experiments (Fig. 4). These changes are attributed to the deposition of organic compounds, as evidenced by the temperature-programmed-oxidation (TPO) tests discussed in the following paragraph. The increase in the average pore width of Al-MCM-41 is explained by the blockage of the smallest pores of the catalyst.

In order to determine the cause of the change in the textural properties of the catalysts, temperature-programme-oxidation (TPO) analysis were carried out. Fig. 6 shows the evolution with temperature of the mass spectrometer signal attributed to CO<sub>2</sub>. A peak appeared at 380 °C for TiO<sub>2</sub> and 530 °C for Al-MCM-41. These results suggest that the compounds adsorbed on the catalyst surface are different for both catalysts. Thus, higher oxidation temperature is typically associated to molecules of large molecular weight, requiring higher activation energy for their oxidation. Previous studies [29,37] have pointed out that deactivation of acid catalysts (like Al-MCM-41) is caused by fouling of acetic acid oligomers, a reaction that generates well-ordered deposits that decompose and oxidize at high temperature. Regarding TiO<sub>2</sub>, deactivation is caused by the adsorption of acetone-derived dimers and trimers, which are desorbed and oxidized at a lower temperature, as shown in Fig. 6. According to the results of the TPO test, the catalyst can be regenerated by oxidation of the adsorbed species.

Table 1  
Textural properties of fresh and used catalysts.

	TiO <sub>2</sub>		Al-MCM-41	
	Fresh	Used (A)	Fresh	Used (A)
BET surface (m <sup>2</sup> /g)	149	86.3	810	273
Pore volume (cm <sup>3</sup> /g)	0.42	0.22	0.77	0.50
Average pore width (nm)	9.6	9.8	4.5	12.8

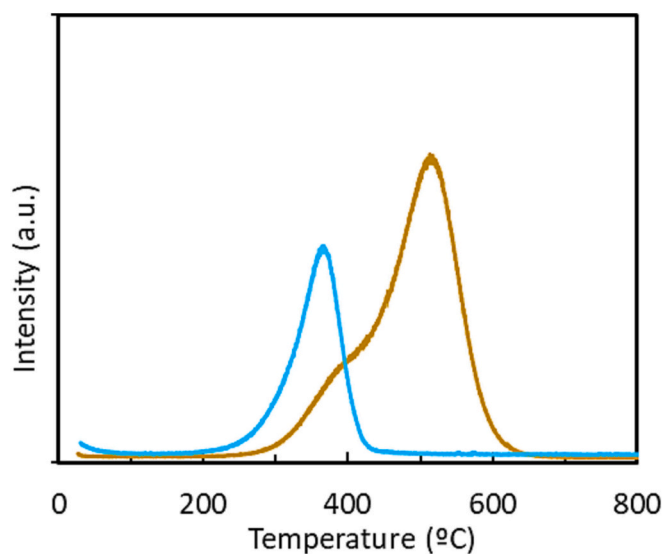


Fig. 6. TPO analysis of used TiO<sub>2</sub> (●) and Al-MCM-41 (●) catalysts.

### 3.4. Reaction mechanism and kinetic model

This section analyzes the mechanism of the different reaction steps depicted in the scheme of Fig. 3. Then, a kinetic model is developed based on this mechanism.

Acetone self-condensation to mesityl oxide (MO) (reaction 1) occurs in a different manner depending on the type of catalyst. Base catalysts are able to abstract the H<sup>α</sup> with formation of a carbanion intermediate, which is stabilized by the enolate resonance isomer [38]. The carbanion then reacts with the carbonyl group of a second acetone molecule and, upon catalyst deprotonation, leads to diacetone alcohol (DAA). Fig. 7 shows the mechanism of the different reaction steps taking place in basic catalysts. This figure has been obtained from findings of the present and previous works from the literature. In these works, the chemical structure of the intermediates has been determined using different techniques, as gas chromatography, mass spectroscopy (GC-MS), diffuse reflectance infrared Fourier transform spectroscopy (DRIFT), and density functional theory calculations (DFT).

When the reaction is conducted at high temperature in the gas phase (like in the present work), the diacetone alcohol dehydrates very rapidly to yield mesityl oxide and isomesityl oxide (IMO) [39,40]. Diacetone alcohol intermediate was not detected in the analysis of the reactor

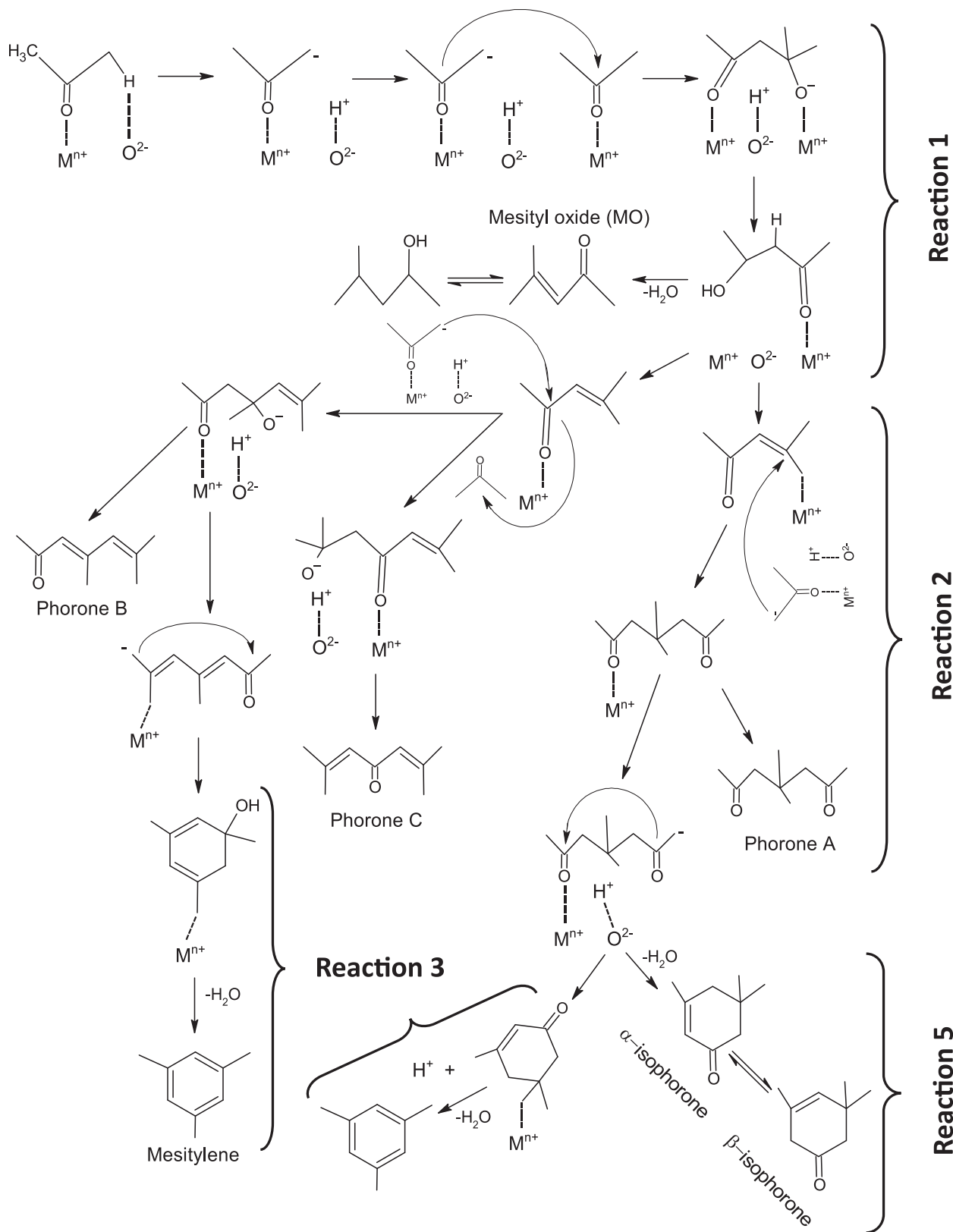


Fig. 7. Reaction mechanism of acetone self-condensation over basic catalysts.

outlet, suggesting the consumption rate of this intermediate is much faster than its formation. Therefore, the reaction between adsorbed acetone and acetone from the gas phase is considered the rate-limiting step of the reaction mechanism. The experiments carried out using mesityl oxide as reactant revealed the presence of acetone as product.

Consequently, this reaction is reversible. Considering that the other reaction steps are in equilibrium and from a balance to the catalyst active sites, the following expressions are obtained for the reaction rate:

$$r_1 = k_1 \theta_A C_A - k_{-1} \theta_{DA} \quad (4)$$

$$r_1 = \frac{k_1 K_A C_A^2 - k_{-1} K_{MO} C_{MO} C_{H_2O}}{1 + K_A C_A + K_{MO} C_{MO}} \quad (5)$$

Where  $\theta_i$  are the adsorbed fractions of compound  $i$ ,  $K_i$  are the adsorption equilibrium constants,  $C_i$  are the molar concentrations, and  $k_j$  are the kinetic constants of reaction  $j$ .

The second step of the reaction scheme consists of phorone generation by condensation of acetone and mesityl oxide (reaction 2). Three different products are possible in this aldol condensation depending on the strength of the basic sites [21]: phorone A (4,4'-dimethylhepta-2,6-di-one), phorone B (2,4-dimethyl-2,4-heptadiene-6-one) and phorone C (2,6-Dimethylhepta-2,5-dien-4-one). When mesityl oxide is adsorbed on

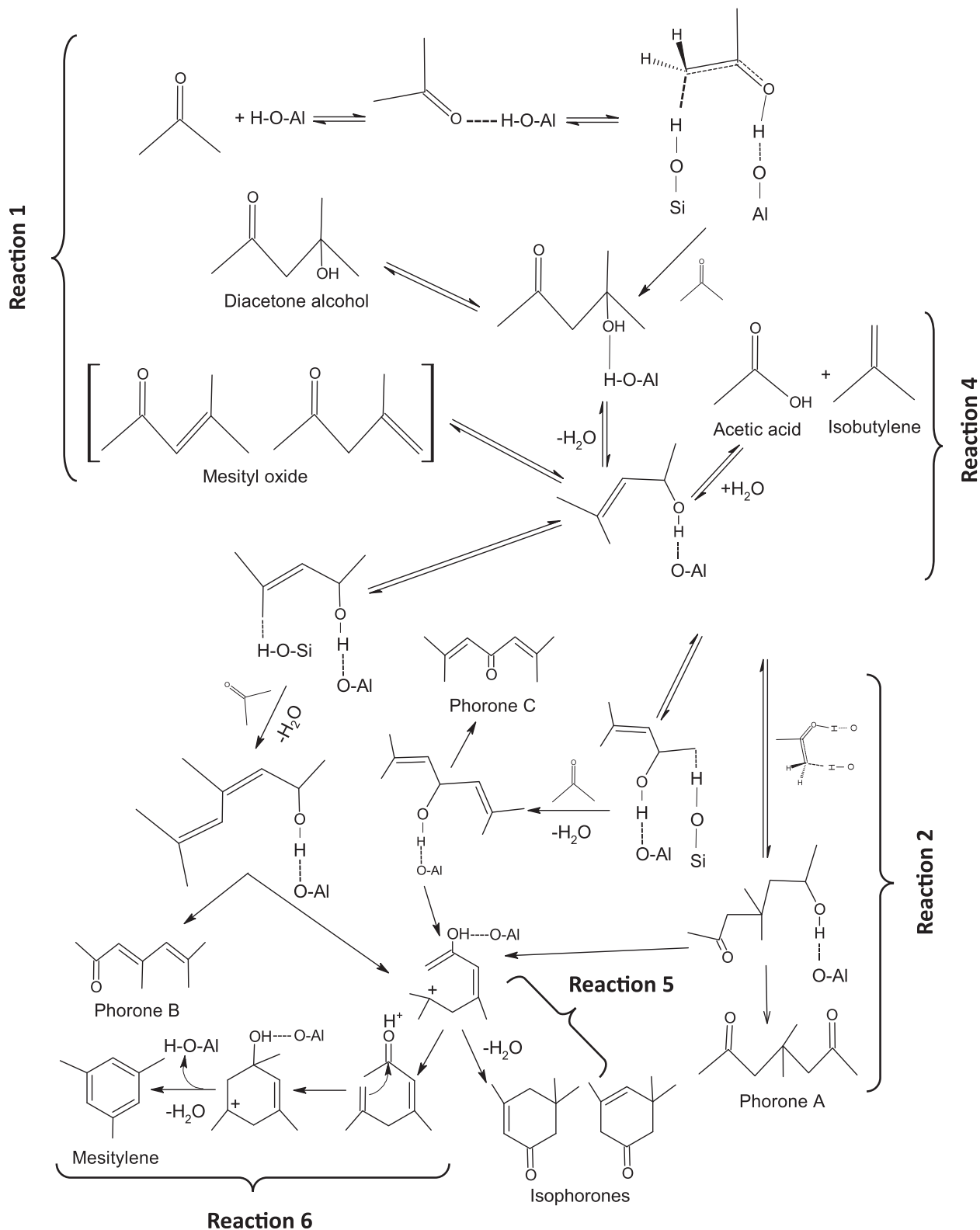


Fig. 8. Reaction mechanism of acetone self-condensation on acid catalysts.

the strongest basic sites and the enolate is formed from acetone adsorbed in a medium-strength basic site, phorone A is generated through the Michael addition mechanism. Conversely, when mesityl oxide and acetone are adsorbed on medium-strength basic sites, phorone B or phorone C are produced by aldol condensation, depending on the enolate precursor, respectively, acetone or mesityl oxide [41]. Assuming the rate-limiting step of the mechanism is the reaction between adsorbed mesityl oxide and acetone from the gas phase, or vice versa, eq. 6 and 7 represent the reaction rate for this step:

$$r_2 = k_2\theta_{MO}C_A \text{ or } r_2 = k_2\theta_A C_{MO} \quad (6)$$

$$r_2 = \frac{k'_2 C_{MO} C_A}{1 + K_A C_A + K_{MO} C_{MO}} \quad (7)$$

Where  $k'_2 = k_2 K_{MO}$  or  $k'_2 = k_2 K_A$ , depending of the prevailing path of mechanism.

Isophorone can be obtained via an internal 1,6-Michael cyclization of adsorbed phorone A using basic catalysts (reaction 5) [38]. Isophorone itself yields no other product, being a stable terminal product in the presence of basic catalysts with strong basic sites (bidentates and monodentates). Mesitylene can be produced with loss of water by 1,6 aldol cyclization of adsorbed phorone B (reaction 3) [39]. The product distribution is affected by the strength of the basic catalysts. If the basicity of the active site is strong, mesityl oxide remains adsorbed and a third acetone molecule will react with the dimer, increasing the selectivity to phorones, isophorone and mesitylene. However, if the strength of the basic site is weak, the formed mesityl oxide desorbs easily and the selectivity to this product is the highest [40].

Finally,  $\beta$ -scission of mesityl oxide to isobutylene and acetic acid (reaction 4) is a lateral, non-desired reaction, because it consumes part of the formed mesityl oxide with a negative impact in mesitylene yield. This reaction is catalyzed by acid sites, specifically the strongest acid sites [29]. However, higher basicity promotes the  $\alpha$ -H abstraction of mesityl oxide to form an enolate, which favors secondary aldolization of acetone to surface phorone intermediate. Followed by a facile decomposition of phorone, the reactions eventually produce isobutene as a major product [33]. According to the experiments performed in the present work with the TiO<sub>2</sub> catalyst, the amount observed of isobutene and acetic acid were very little. Hence, this reaction step can be considered negligible.

On acid catalysts, acetone self-condensation (reaction 1) takes place according to a different mechanism, as depicted in Fig. 8. First, an acetone molecule interacts with the acid site forming an H-bond. After that, a tautomerization of the molecule takes place, and it reacts with another acetone molecule from the gas phase. This is the rate-limiting step of the reaction mechanism. Three different products are possible: diacetone alcohol (DAA), mesityl oxide (MO) and isomesityl oxide (IMO). DAA is not observed in the reactor effluent, so it can be considered that the decomposition rate is faster than the formation rate, as with the basic catalyst. MO and IMO production involves a dehydration step [31,42].

The Lewis sites of the acid catalyst improve the yield of phorone (reaction 2) and isophorone (reaction 5) production [43]. Previous studies with acid catalysts [26] showed that mesitylene can be produced via isophorone dehydration and rearrangement (reaction 6) [32] and that the routes involving dehydration-cyclization of linear phorones are negligible (reaction 3). The lower dehydration capacity of basic catalysts explains the lower mesitylene yield these catalysts when compared with acid catalysts.

The  $\beta$ -scission of mesityl oxide to isobutylene and acetic acid (reaction 4) is an important reaction in acid catalyst, as evidenced by the selectivity to these compounds obtained experimentally (Fig. 5). The reaction mechanism proceeds as follows: mesityl oxide produced from acetone condensation is protonated and, then, decomposes into a surface acetate and isobutene. Acetic acid is finally generated by hydration and

desorption of this acetate [30]. The kinetic equation of this reaction step can be obtained from the mechanism considering the decomposition of mesityl oxide as the rate-limiting step:

$$r_4 = k_4\theta_{MO} \quad (8)$$

$$r_4 = \frac{k'_4 C_{MO}}{1 + K_A C_A + K_{MO} C_{MO}} \quad (9)$$

### 3.5. Fitting of the kinetic model: Effect of concentration on reaction rate

The experiments of this section were aimed at measuring the reaction rate at different concentration, to fit the kinetic models proposed in the previous section. Two set of experiments were conducted. First, acetone feed concentration was varied in the range 5–20% (mole). Then, feeds consisting of a mixture of acetone and mesityl oxide at 1:1 and 3:1 ratio were used (1–5% of mesityl oxide and 3–15% of acetone). Pressure and temperature were kept constant at 250 kPa and 240 °C.

Reaction rates of reactants and products were calculated using eq. (3), assuming differential conditions in the fixed-bed reactor (e.g., same concentration for all the catalyst particles). To fulfill this requirement, the space time (WHSV) was adjusted to ensure conversion was kept below 10% at each tested condition. For TiO<sub>2</sub>, the space time was 7900 mol/kg h for acetone alone as reactant and 1900 mol/kg h for the mixture of acetone and mesityl oxide. Conversely, for Al-MCM-41, the space time were 5000 and 1400 mol/kg h, respectively, for acetone alone and acetone/mesityl oxide mixtures. The rates of the individual steps of the reaction scheme (depicted in Fig. 2) were calculated using the stoichiometry of these reactions.

The results are summarized in Fig. 9 for TiO<sub>2</sub> and Fig. 10 for Al-MCM-41. For all the cases, the increase of concentration of the corresponding reactant caused an increase in reaction rate.

The results of acetone condensation to mesityl oxide (reaction 1) were obtained using acetone alone as reactant. As observed for both catalysts, reaction rate has a strong dependence on acetone concentration of almost second order. At high acetone concentration, this dependence is attenuated, attributed to competitive adsorption of acetone, as predicted by eq. (5). Using these experimental data, the direct kinetic constant ( $k_1$ ) and acetone adsorption constant ( $K_A$ ) of eq. (5) were calculated, as reported in Table 2. Acetone adsorption constant was similar for both catalyst, 0.37 and 0.42 m<sup>3</sup>/mol, respectively, for TiO<sub>2</sub> and Al-MCM-41.

The other steps of the reaction scheme were studied using a feed made of mixtures of acetone and mesityl oxide. For the TiO<sub>2</sub> catalyst, the condensation of mesityl oxide to phorone (reaction 2) was found to be of first order with respect to mesityl oxide and acetone concentration (Fig. 7b), which fits the kinetic equation proposed from the reaction mechanism, eq. (7). This was checked in validation experiments carried out with a different acetone to mesityl oxide ratio (1:1 and 3:1). Competitive adsorption of mesityl oxide had a negligible influence on reaction rate ( $K_{MO}C_{MO} \approx 0$ ) for this catalyst. Conversely, for the Al-MCM-41 catalyst, competitive adsorption of mesityl oxide was observed for both reactions, involving this compound as reactant: the condensation to phorones (reaction 2) and the  $\beta$ -scission (reaction 4). In these reactions, the increase of reaction rate was reduced at high MO concentrations. The fitted MO adsorption constant was 48.9 m<sup>3</sup>/mol.

The phorones dehydration steps, leading to the formation of mesitylene (reaction 3) or isophorone (reaction 5) and the further isophorone dehydration to mesitylene, were fitted to simple first order kinetic equations, as evidenced by the experiments reported in Figs. 9 and 10.

The quality of the fitting can be assessed using the correlation coefficients R<sup>2</sup> of Table 2 and the parity plot of Fig. 11, where model predicted reaction rates are depicted as a function of the experimental ones. Overall, it can be said that the models are able of predicting the kinetics of the complex reaction scheme of acetone self-condensations. The proposal of such a complete model can contribute to the scale-up

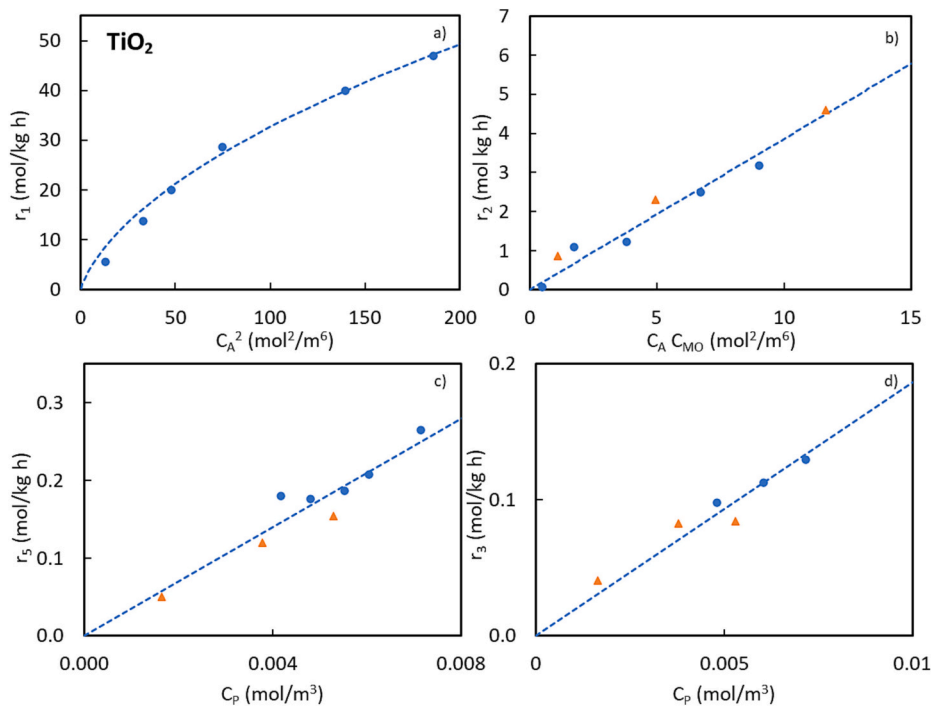


Fig. 9. Influence of concentration on reaction rate for the TiO<sub>2</sub> catalyst: acetone alone (a), acetone to mesityl oxide ratio of 1:1 (●) and 3:1 (▲) (b, c, d).

of the reaction and to select the most appropriate catalyst.

### 3.6. Dependence of temperature

The influence of temperature was studied in the range of 240–340 °C, as higher temperatures had a clearly negative impact in the reaction, due to the oligomerization of acetone or coke formation, related to catalyst deactivation.

The objective of this set of experiments was determining the influence of temperature in product distribution for both catalysts and determining the activation energy for the different reaction steps.

As it can be seen in Fig. 12, product selectivity distribution is different with respect to the selectivity values observed during the stability studies performed at 275 °C (Figs. 4 and 5). This can be due to modifications in the catalyst occur during the studies performed in-between.

An increase of temperature showed a positive impact for TiO<sub>2</sub> with an increase of conversion and, up to 275 °C, also mesityl oxide selectivity. Above 275 °C, mesityl oxide selectivity remained constant or decreased slightly, while mesitylene, phorone and isophorone selectivity increased. This change agrees with an increase of conversion, leading to an increase of selectivity of the intermediates and final products.

The behavior of the Al-MCM-41 catalyst with temperature is quite different. Though acetone conversion increased with temperature, the impact on selectivity was negative, because of favoring the  $\beta$ -scission reaction. Thus, isobutylene selectivity increased considerably with temperature, while mesityl oxide selectivity decreased.

The rates of the different steps of the reaction scheme were determined at each temperature and the corresponding kinetics constants were obtained using the kinetic equations determined previously. Fig. 13 depicts the Arrhenius plot for the kinetic constants, from which the activation energy was calculated, as reported in Table 2.

It can be noticed that temperature has a low influence for some of the reaction steps, especially reactions 5 and 6 that have low activation energies (< 20 kJ/mol). Conversely, the decomposition of mesityl oxide to isobutylene and acetic acid (reaction 4, being only important for the Al-MCM-41 catalyst) is the reaction with the highest influence of

temperature (activation energy of 72.4 kJ/mol). This means that an increase in temperature will favor this reaction among the others, as observed in the increase of isobutylene selectivity of Fig. 12a. The activation energies of the acetone condensation steps (reactions 1 and 2) are quite similar for both catalysts, in the range 36–48 kJ/mol.

As explained above, temperature must be selected carefully for these catalysts to control product distribution and direct it to the desired species. The most critical catalyst regarding temperature is Al-MCM-41 with an optimum temperature to maximize mesitylene yield of ca. 250–275 °C. The TiO<sub>2</sub> catalyst performs well within this temperature range. This means that both catalysts can be combined as a mechanical mixture in a single reactor, as proposed in a previous work [29]. The findings of the present work, regarding the reaction kinetics of the catalysts, are very useful to suggest a recommended arrangement for the scale-up of the process. This arrangement is based on two consecutive fixed beds: the bed placed upstream made of TiO<sub>2</sub> and the bed placed downstream made of Al-MCM-41. The first bed would convert part of acetone to mesityl oxide and phorone, while the second bed would complete the condensation and dehydration reactions to mesitylene. Also, by adjusting the reactor per-pass conversion, selectivity to the undesired isobutylene product can be controlled. The performance of this set-up will be addressed in future works with this reaction.

### 3.7. Assessment of mass transfer limitations

The occurrence of mass transfer limitations was evaluated at the highest concentration (15% acetone) and temperature (340 °C), conditions leading to the highest reaction rates.

Carberry number was used to evaluate the relative importance of external mass transport to reaction rate, eq. (10). Values of 0.031 and 0.047 were obtained, respectively, for TiO<sub>2</sub> and Al-MCM-41, which fall below 0.05, so this mass transport resistance can be neglected.

$$Ca = \frac{r_{obs} \rho_{cat}}{a k_f C_{Ab}} < 0.05 \quad (10)$$

Where  $r_{obs}$  is the observed reaction rate,  $a$  is the specific external surface area for the catalyst particles,  $k_f$  is the mass transfer coefficient,

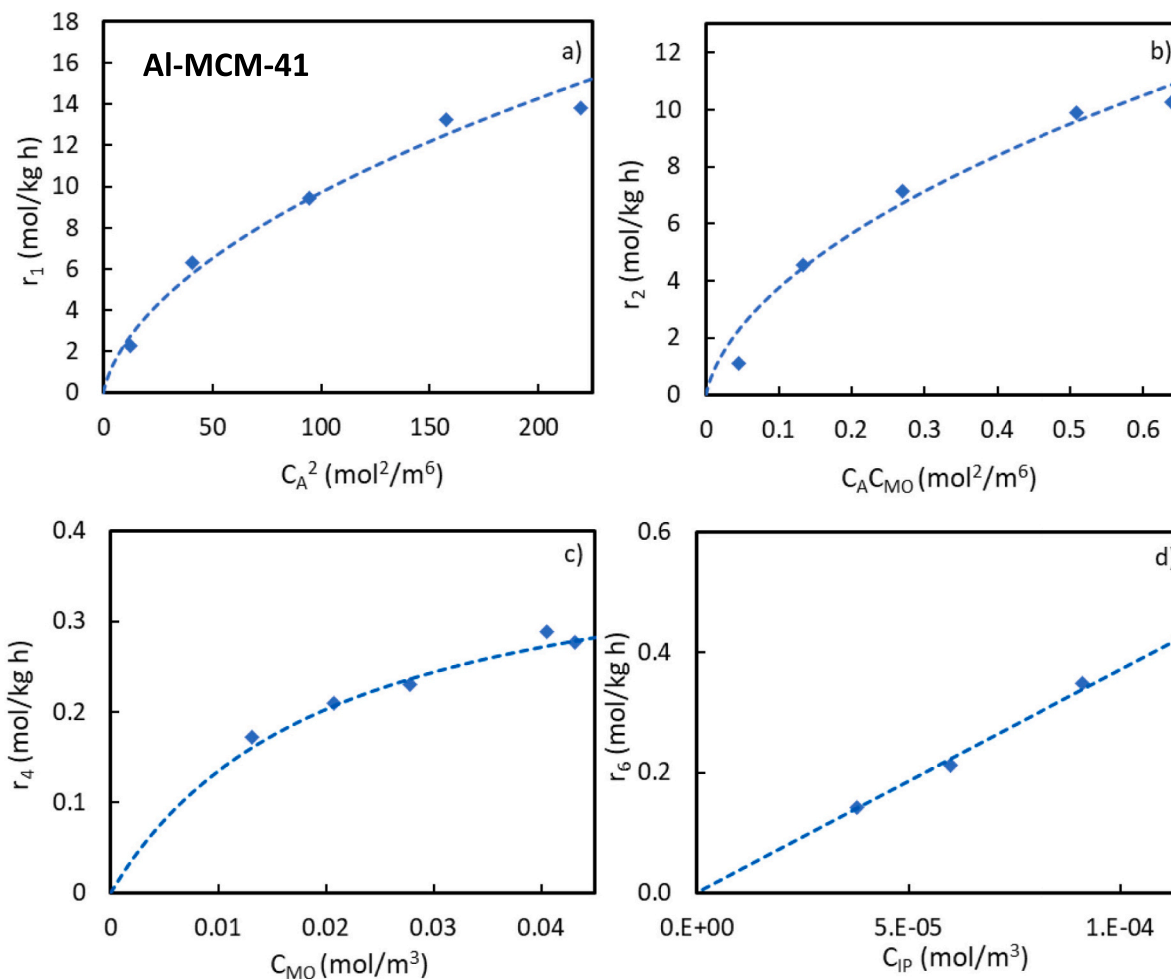


Fig. 10. Influence of concentration on reaction rate for the Al-MCM-41 catalyst: acetone alone (a, b, c), acetone to mesityl oxide ratio of 1:1 (d).

Table 2

Fitting parameters of the kinetic model for the TiO<sub>2</sub> and Al-MCM-41 catalysts.

Parameter	TiO <sub>2</sub>			Al-MCM-41		
	Constant at 240 °C	E <sub>a</sub> (kJ/mol)	R <sup>2</sup>	Constant at 240 °C	E <sub>a</sub> (kJ/mol)	R <sup>2</sup>
k <sub>1</sub> (m <sup>3</sup> /kg h)	4.15	38.1	0.950	1.2	41.8	0.988
k <sub>2</sub> ' (m <sup>6</sup> /kg h mol)	0.39	44.4	0.991	58.6	36.1	0.998
k <sub>3</sub> (m <sup>3</sup> /kg h)	18.6	42.1	0.992	–	–	–
k <sub>4</sub> (mol/kg h)	–	–	–	0.41	72.4	0.998
k <sub>5</sub> (m <sup>3</sup> /kg h)	34.9	17.4	0.996	–	–	–
k <sub>6</sub> (m <sup>3</sup> /kg h)	–	–	–	3712	18.4	0.999
K <sub>A</sub> (m <sup>3</sup> /mol)	0.37	–	0.992	0.42	–	–
K <sub>MO</sub> (m <sup>3</sup> /mol)	–	–	–	48.9	–	–

and  $c_b$  is the reactant concentration in the gas.

Pore diffusion limitations were evaluated using Wheeler-Weisz modulus, eq. (11), with values of  $1.8 \cdot 10^{-4}$  and  $5.2 \cdot 10^{-3}$ , respectively, for TiO<sub>2</sub> and Al-MCM-41. Since these values are smaller than 0.15, internal or pore diffusion was not a limitation for the reaction rate [44].

$$\phi = \left( \frac{r_{obs} \rho_{cat} L^2}{D_e c_{As}} \right) \left( \frac{n+1}{2} \right) < 0.15 \quad (11)$$

Where  $L$  is the characteristic length of the catalyst particles,  $D_e$  is the effective diffusivity inside the catalyst pore network,  $c_s$  is the reactant concentration at particle surface, and  $n$  is the reaction order.

#### 4. Conclusions

Acetone self-condensation to mesitylene catalyzed by acid (Al-MCM-41) and basic (TiO<sub>2</sub>) catalysts has been studied in a gas-phase continuous fixed-bed reactor. It has been found that both catalysts deactivate during the first hours of reaction, due to the blockage of the strongest active sites by formation of acetone oligomers and coke. After this initial deactivation, conversion was stable, and the catalyst kept part of the initial activity. The reaction kinetics of the individual steps of the reaction scheme was determined in experiments planned at different feed concentrations and temperatures. The gathered data was used to fit a complex mechanistic kinetic model for the first time for this reaction and the studied catalysts. A second order reaction kinetics was confirmed for

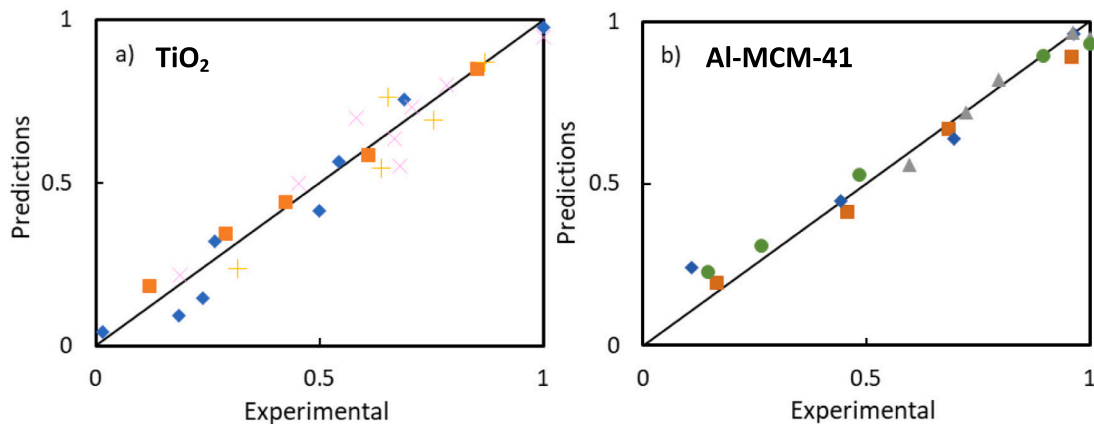


Fig. 11. Parity plot of model predicted reaction rates as a function of the experimental one for TiO<sub>2</sub> (a) and Al-MCM-41 (b) catalysts. Reactions:  $\square$  r<sub>1</sub>,  $\diamond$  r<sub>2</sub>,  $+$  r<sub>3</sub>,  $\blacktriangle$  r<sub>4</sub>,  $\times$  r<sub>5</sub> and  $\bullet$  r<sub>6</sub>.

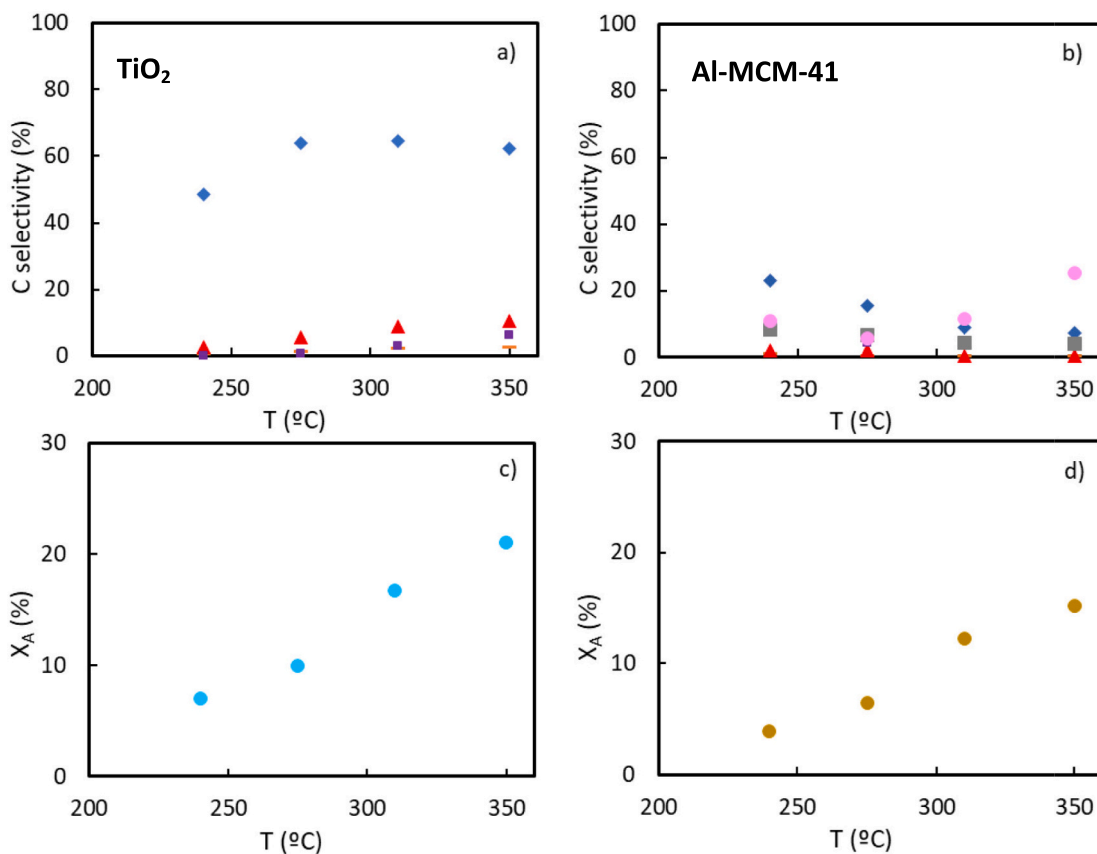


Fig. 12. Product selectivity distribution and conversion as a function of temperature for TiO<sub>2</sub> (a, c) and Al-MCM-41 (b, d) catalysts. Legend: Mesityl oxide ( $\diamond$ ), phorone ( $-$ ), isophorone ( $\blacktriangle$ ), mesitylene ( $\blacksquare$ ), isobutylene ( $\bullet$ ) are represented.

acetone self-condensation to mesityl oxide, the first step of the reaction scheme, with activation energies of 38.1 and 41.8 kJ/mol, respectively for TiO<sub>2</sub> and Al-MCM-41 catalysts.

It can be concluded that, the most important drawback of the acid Al-MCM-41 catalyst is the undesired reaction of mesityl oxide decomposition to isobutylene and acetic acid, which reduces mesitylene yield

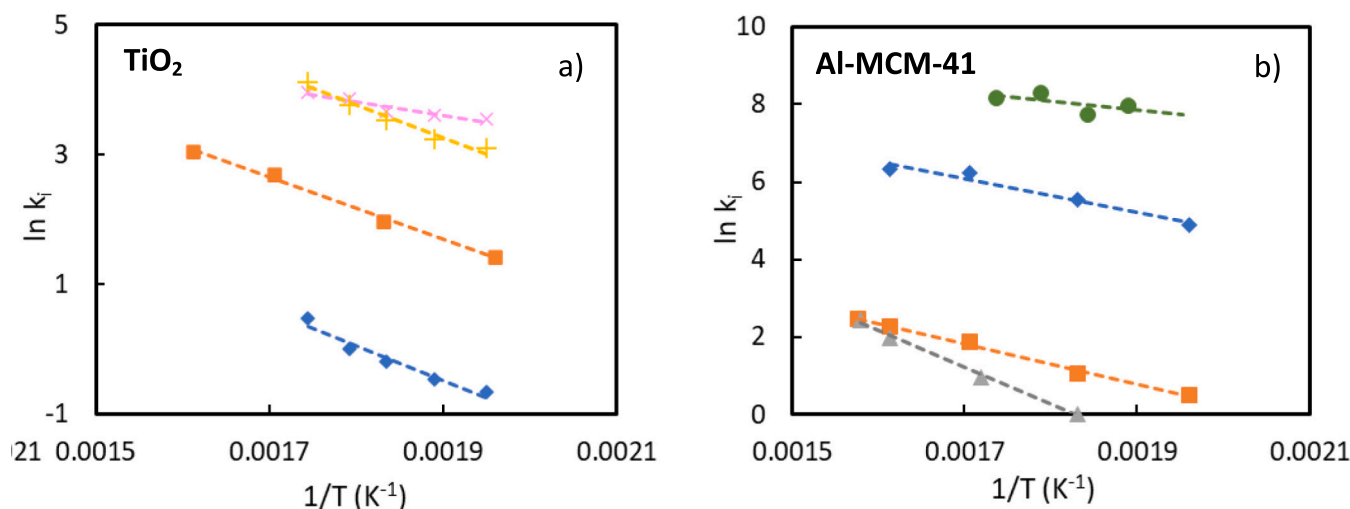


Fig. 13. Arrhenius plot for TiO<sub>2</sub> (a) and Al-MCM-41 (b) catalysts.

Reactions: ■ r<sub>1</sub>, ◆ r<sub>2</sub>, + r<sub>3</sub>, ▲ r<sub>4</sub>, × r<sub>5</sub> and ● r<sub>6</sub>.

considerably. Conversely, the basic character of TiO<sub>2</sub> catalyst did not catalyze this acid-catalyzed side reaction, isophorone was the main product. Hence, it is proposed that a combination of both catalysts can be interesting to increase mesitylene yield. For this purpose, the kinetic model developed in the present work is a valuable tool to assess the optimum mixture and operating conditions.

#### CRediT authorship contribution statement

**Adrián García:** Investigation, Writing – original draft. **Pablo Marín:** Methodology, Supervision, Validation, Writing – review & editing. **Salvador Ordóñez:** Conceptualization, Supervision, Writing – review & editing, Funding acquisition.

#### Declaration of Competing Interest

The authors declare that they have no known competing financial interests or personal relationships that could have appeared to influence the work reported in this paper.

#### Data availability

Data will be made available on request.

#### Acknowledgements

This work has been funded by the Spanish Ministry of Science and Innovation, Spanish Agency for Research AEI (PDC-2021-120835-C21, BIOMODCAT-PoC).

Adrian Garcia also thanks for his Ph.D. fellowship (PA-22-BP21-016) of the Severo Ochoa Program of the local Government of the Principality of Asturias.

#### References

- J.H. Clark, T.J. Farmer, L. Herrero-Davila, J. Sherwood, Circular economy design considerations for research and process development in the chemical sciences, *Green Chem.* 18 (2016) 3914–3934.
- P. Reif, N.K. Gupta, M. Rose, Highly stable amorphous silica-alumina catalysts for continuous bio-derived mesitylene production under solvent-free conditions, *Green Chem.* 25 (2023) 1588–1596.

- International Energy Agency (IEA), in, 2023. <https://www.iea.org/energy-system/transport/aviation>.
- J. Han, A. Elgowainy, H. Cai, M.Q. Wang, Life-cycle analysis of bio-based aviation fuels, *Bioresour. Technol.* 150 (2013) 447–456.
- P. Gegg, L. Budd, S. Ison, The market development of aviation biofuel: Drivers and constraints, *J. Air Transp. Manag.* 39 (2014) 34–40.
- A. Elgowainy, J. Han, M. Wang, N. Carter, R. Stratton, J. Hileman, A. Malwitz, S. Balasubramanian, Life-cycle analysis of alternative aviation fuels in GREET, in: Argonne National Lab.(ANL), Argonne, IL (United States), 2012.
- R. Stratton, H.M. Wong, J. Hileman, Life cycle greenhouse gas emissions from alternative jet fuels, in: Partnership for Air Transportation Noise and Emissions Reduction, 2010.
- A. Burnham, J. Han, C.E. Clark, M. Wang, J.B. Dunn, I. Palou-Rivera, Life-cycle greenhouse gas emissions of shale gas, natural gas, coal, and petroleum, *Environ. Sci. Technol.* 46 (2012) 619–627.
- J.B. Dunn, S. Mueller, H.-Y. Kwon, M.Q. Wang, Land-use change and greenhouse gas emissions from corn and cellulosic ethanol, *Biotechnol. Biofuels* 6 (2013) 1–13.
- J. Han, A. Elgowainy, J.B. Dunn, M.Q. Wang, Life cycle analysis of fuel production from fast pyrolysis of biomass, *Bioresour. Technol.* 133 (2013) 421–428.
- P. Zhao, S. Han, X. Li, T. Zhu, X. Tao, L. Guo, Comparison of RP-3 pyrolysis reactions between surrogates and 45-component model by ReaxFF molecular dynamics simulations, *Energy Fuel* 33 (2019) 7176–7187.
- E.R. Sacia, M. Balakrishnan, M.H. Deaner, K.A. Goulas, F.D. Toste, A.T. Bell, Highly selective condensation of biomass-derived methyl ketones as a source of aviation fuel, *ChemSusChem* 8 (2015) 1726–1736.
- Y.-Y. Chen, Z. Wei, S. Wang, J. Li, M. Dong, Z. Qin, J. Wang, H. Jiao, W. Fan, Kinetics and thermodynamics of polymethylbenzene formation over zeolites with different pore sizes for understanding the mechanisms of methanol to olefin conversion—a computational study, *Catalysis Sci. Technol.* 6 (2016) 5326–5335.
- G. Booth, Nitro compounds, aromatic, Ullmann's encyclopedia of industrial chemistry, 2000.
- J. Trotter, The crystal structures of some mesitylene and duren derivatives. II. Nitromesitylene, *Acta Crystallogr.* 12 (1959) 605–607.
- S. Sharma, M.S. Hundal, N. Singh, G. Hundal, Nanomolar fluorogenic recognition of Cu (II) in aqueous medium—a highly selective “on-off” probe based on mesitylene derivative, *Sensors Actuators B Chem.* 188 (2013) 590–596.
- J.J. McKetta Jr., *Encyclopedia of Chemical Processing and Design*, CRC Press, 1997.
- M.I. Al-Zeer, K.J. MacKenzie, Fly ash-based geopolymers as sustainable bifunctional heterogeneous catalysts and their reactivity in Friedel-Crafts acylation reactions, *Catalysts* 9 (2019) 372.
- G.S. Harold W. Earhart, Alkylation and isomerization process, US3542890A, in: K. I. Inc (Ed.), US, 1969.
- T. Imai, US 4 487 984, in: U.O. Products (Ed.), US, 1984.
- G. Salvapati, K. Ramanamurthy, M. Janardanao, Selective catalytic self-condensation of acetone, *J. Mol. Catal.* 54 (1989) 9–30.
- V. Zakoshansky, The cumene process for phenol-acetone production, *Pet. Chem.* 47 (2007) 273–284.
- N. Qureshi, T.C. Ezeji, Butanol, a superior biofuel production from agricultural residues (renewable biomass): recent progress in technology, *Biofuels, Bioproducts and Biorefining: Innovation for a sustainable economy 2* (2008) 319–330.

- [24] D. Mansur, T. Yoshikawa, K. Norinaga, J.-I. Hayashi, T. Tago, T. Masuda, Production of ketones from pyrolytic acid of woody biomass pyrolysis over an iron-oxide catalyst, *Fuel* 103 (2013) 130–134.
- [25] M.N. Abbas, S.A. Ibrahim, Z.N. Abbas, T.A. Ibrahim, Eggshells as a sustainable source for acetone production, *J. King Saud Univ. Eng. Sci.* 34 (2022) 381–387.
- [26] J. Quesada, L. Faba, E. Díaz, S. Ordóñez, Effect of catalyst morphology and hydrogen co-feeding on the acid-catalysed transformation of acetone into mesitylene, *Catalysis Sci. Technol.* 10 (2020) 1356–1367.
- [27] Z. Wu, J. Zhang, Z. Su, S. Lu, J. Huang, Y. Liang, T. Tan, F.-S. Xiao, Selective conversion of acetone to mesitylene over tantalum phosphate catalysts, *Chem. Commun.* 58 (2022) 2862–2865.
- [28] S. Taco-Vasquez, M.T. Holtzapfle, Conversion of acetone and mixed ketones to hydrocarbons using HZSM-5 catalyst in the carboxylate platform, *PLoS One* 17 (2022), e0277184.
- [29] L. Faba, J. Gancedo, J. Quesada, E. Diaz, S. Ordóñez, One-pot conversion of acetone into mesitylene over combinations of acid and basic catalysts, *ACS Catal.* 11 (2021) 11650–11662.
- [30] P. Huber, P.N. Plessow, A computational investigation of the decomposition of acetic acid in H-SSZ-13 and its role in the initiation of the MTO process, *Catalysis Sci. Technol.* 13 (2023) 1905–1917.
- [31] S. Herrmann, E. Iglesia, Elementary steps in acetone condensation reactions catalyzed by aluminosilicates with diverse void structures, *J. Catal.* 346 (2017) 134–153.
- [32] V.S. Kumar, B. Nagaraja, V. Shashikala, P. Seetharamulu, A. Padmasri, B.D. Raju, K.R. Rao, Role of acidic and basic sites of Al<sub>2</sub>O<sub>3</sub> in predicting the reaction pathway of isophorone transformation, *J. Mol. Catal. A Chem.* 223 (2004) 283–288.
- [33] H. Li, J. Sun, Y. Wang, Surface acetone reactions on Zn<sub>x</sub>Zr<sub>y</sub>O<sub>z</sub>: a DRIFTS-MS study, *Appl. Catal. A Gen.* 573 (2019) 22–31.
- [34] J.I. Di Cosimo, C.R. Apesteguía, Study of the catalyst deactivation in the base-catalyzed oligomerization of acetone, *J. Mol. Catal. A Chem.* 130 (1998) 177–185.
- [35] M. Zamora, T. López, R. Gómez, M. Asomoza, R. Meléndrez, Acetone gas phase condensation on alkaline metals doped TiO<sub>2</sub> sol–gel catalysts, *Appl. Surf. Sci.* 252 (2005) 828–832.
- [36] C. Perego, S. Peratello, Experimental methods in catalytic kinetics, *Catal. Today* 52 (1999) 133–145.
- [37] J. Quesada, L. Faba, E. Díaz, S. Bennici, A. Auroux, S. Ordóñez, Role of surface intermediates in the deactivation of MgZr mixed oxides in acetone self-condensation: a combined DRIFT and ex situ characterization approach, *J. Catal.* 329 (2015) 1–9.
- [38] J. Di Cosimo, V. Díez, C. Apesteguía, Base catalysis for the synthesis of  $\alpha$ ,  $\beta$ -unsaturated ketones from the vapor-phase aldol condensation of acetone, *Appl. Catal. A Gen.* 137 (1996) 149–166.
- [39] W. Reichle, Pulse microreactor examination of the vapor-phase aldol condensation of acetone, *J. Catal.* 63 (1980) 295–306.
- [40] M. Zamora, T. López, R. Gómez, M. Asomoza, R. Meléndrez, Oligomerization of acetone over titania-doped catalysts (Li, Na, K and Cs): effect of the alkaline metal in activity and selectivity, *Catal. Today* 107 (2005) 289–293.
- [41] L. Faba, E. Díaz, S. Ordóñez, Gas phase acetone self-condensation over unsupported and supported Mg–Zr mixed-oxides catalysts, *Appl. Catal. B Environ.* 142 (2013) 387–395.
- [42] A. Panov, J. Fripiat, Acetone condensation reaction on acid catalysts, *J. Catal.* 178 (1998) 188–197.
- [43] M. Konieczny, G. Sosnovsky, Novel aspects in the preparation of phorone, *Zeitschrift für Naturforschung B* 33 (1978) 454–460.
- [44] J. Pérez-Ramírez, R.J. Berger, G. Mul, F. Kapteijn, J.A. Moulijn, The six-flow reactor technology: a review on fast catalyst screening and kinetic studies, *Catal. Today* 60 (2000) 93–109.